ChemPubSoc Europe

DOI: 10.1002/cctc.201900795

CHEMCATCHEM Full Papers

Carbidisation of Pd Nanoparticles by Ethene Decomposition with Methane Production

Wilm Jones,[a, b] Peter. P. Wells,[a, c, d] Emma K. Gibson,[a, e] Arunabhiram Chutia,[a, f] Ian P. Silverwood,[g] C. Richard A. Catlow,[a, b] and Michael Bowker*[a, b]

In the presence of oxygenated organic molecules pure Pd, which is widely used in chemicals processing and the pharmaceutical industry, tends to defunctionalise and dehydrogenate such molecules to H_2, CO and surface/bulk carbon, in the form of a palladium carbide. We have investigated the formation of this carbide by ethene adsorption using a variety of techniques, including pulsed flow reaction measurements, XAS and DFT calculations of the lattice expansion during carbidisation. These experiments show that two main reactions take place above 500 K, that is, both total dehydrogenation, but also disproportionation to methane and the carbide, after which the activity of the Pd is completely lost. We estimate the value of x in PdC_x to be 0.28 (±0.03), and show by computer modelling that this fits the lattice expansion observed by XAFS, and that there is charge transfer to C from Pd of around 0.2–0.4 e.

Introduction

Pd is an important catalytic metal and it is used in a variety of processes, for instance, in the Wacker process for the selective oxidation of ethane to acetaldehyde, in vinyl acetate synthesis and in a wide range of fine chemicals hydrogenation reactions, which are often heterogeneous, liquid phase processes. The interaction of ethylene, ethanol, acetic acid and many other simple organic molecules with the surface of Pd can lead to the formation of palladium carbide.[1–18] This can have an effect on the activity and selectivity of the reaction of interest. To explore this further we have prepared Pd-SiO_2 catalysts and have carried out a seemingly simple reaction, namely ethene decomposition to form PdC_x, and have measured both the uptake of carbon and the lattice expansion of the Pd nanoparticles due to the carbon by X-ray absorption fine structure (XAFS) analysis.

XAFS measurements, either assessing the extended X-ray absorption fine structure (EXAFS) or the X-ray absorption near edge structure (XANES) has proved a crucial tool in determining the structural properties of carbidic and other interstitial Pd systems.[19] Early work by McCaulley performed EXAFS studies of the *in situ* formation of PdC_x by treating supported Pd nanoparticles with ethene at 150 °C.[9,10] This study showed that the formation of PdC_x resulted in an expanded Pd–Pd distance of 2.80 Å, which was ascribed to $PdC_{0.13}$. This stoichiometry was based on the assumption that this was the maximum value of carbon incorporation achievable. More recently, efforts have focussed on using the XANES to discriminate between carbidic and hydridic forms of Pd; the formation of PdC_x results in a broadening and a shift in position (+1 eV) of the main edge transition.[6,18] The features of carbidic and hydridic Pd are readily apparent in the XANES difference spectra (e.g. PdC_x-Pd^0) with characteristic features that allow them to be readily distinguished.[6,7] Furthermore, simulations of these difference spectra have suggested that the value of carbon incorporation could well exceed the value of 0.13.[8]

In our work we have observed that there are different processes occurring during the formation of PdC_x. Surprisingly, together with dehydrogenation, and in contrast with the behaviour of single crystal Pd,[4,18] we find that disproportionation of ethene to carbide and methane is a major reaction pathway. The stoichiometry of the carbide phase has been variously reported from a value of $PdC_{0.05}$[7] to $PdC_{0.16}$[13] (though

[a] W. Jones, P. P. Wells, E. K. Gibson, A. Chutia, C. R. A. Catlow, M. Bowker
UK Catalysis Hub
Research Complex at Harwell
Oxfordshire, OX11 0FA (United Kingdom)
[b] W. Jones, C. R. A. Catlow, M. Bowker
Cardiff Catalysis Institute
School of Chemistry
Cardiff University
Cardiff CF10 3AT (United Kingdom)
[c] P. P. Wells
Diamond Light Source Ltd
Harwell Science & Innovation Campus
Didcot, Oxfordshire, OX11 0DE (United Kingdom)
[d] P. P. Wells
School of Chemistry
University of Southampton
Southampton, SO17 1BJ, (United Kingdom)
[e] E. K. Gibson
School of Chemistry
Joseph Black Building
University of Glasgow
Glasgow, G12 8QQ, (United Kingdom)
[f] A. Chutia
School of Chemistry
Brayford Pool
University of Lincoln
Lincoln LN6 7TS (United Kingdom)
[g] I. P. Silverwood
ISIS Neutron and Muon Facility
Science and Technology Facilities Council
Rutherford Appleton Laboratory
Harwell Science and Innovation Campus
Oxon OX11 0QX, (United Kingdom)

Supporting information for this article is available on the WWW under https://doi.org/10.1002/cctc.201900795

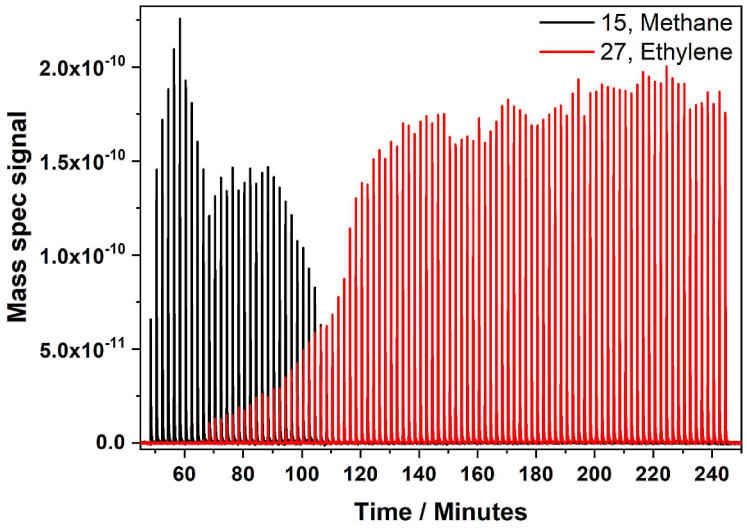

Figure 1. Methane evolution during pulsing ethene over the Pd/SiO_2 catalyst at 300 °C. The evolution is complete after about 32 pulses, and ethene starts to break through after about 10 pulses.

higher levels are reported in the surface regions[6]), but here we find the loading of the carbide to be much higher at ~28 atom% C.

Results and Discussion

As we have shown earlier carbide can be formed in pure Pd crystals[1,2,4] and Pd nanoparticles[3] by treatment in a wide variety of organic molecules. In this work we have used ethene as carbiding agent, a process which is, in principle, very simple. This was certainly shown to be the case by us on well-defined single crystal surfaces, both Pd(110)[4] and (111).[3] However, when we study this reaction carefully in a pulsed flow micro-reactor at much higher pressures, using a supported catalyst, we find something rather different, as shown in Figure 1. Here the main reaction is a kind of disproportionation reaction in which the products are methane and carbide (reaction 2), [Eq. (1) and (2)].

$$(x/2)C_2H_4 + Pd \rightarrow PdC_x + xH_2 \quad (1)$$

$$(x)C_2H_4 + Pd \rightarrow PdC_x + xCH_4 \quad (2)$$

For clarity Figure 1 shows just the methane evolution at 300 °C, but the other product, hydrogen is also shown in Figure S1. It can be seen though that the evolution is rather complicated, with initial hydrogen production, followed by a decrease and coincidently increasing methane. Ethene begins to break through the end of the reactor after about 10 pulses and none is converted after about 120 mins, at which point hydrogen and methane evolution have ceased. More detailed discussion is given in the supplementary information.

Immediately following this experiment, another titration was carried out, this time removing the C using oxygen pulses and the results are shown in Figure S1. Here the titration is clearly much more precise with only CO_2 being evolved for the first 64 pulses, with all the oxygen in the pulse being consumed, followed by a sharp breakthrough of O_2, and dramatic decline in CO_2, which gives us an accurate measure of the carbon deposited into the sample under these conditions, since each pulse contains 4×10^{-7} mol and so the uptake was 2.7×10^{-5} mol of O_2. The total molecular oxygen uptake is equal to the CO_2 evolved, indicating the simple clean-off ($C+O_2\rightarrow CO_2$). The same is seen on single crystals, with all adsorbed oxygen being evolved as CO_2 until the C is used up.[18] We estimate the value of x in PdC_x to be 0.25 (±0.03) the calculation of this number is shown in the supplementary material.

Structural measurements were also made on the catalyst. TEM measurements indicate that the average size of particles is 7 nm, with a median of 5 nm (Figure S2). We have used XRD and XAS to investigate changes in the structure during reaction. We find that the Pd diffraction peak shifts after carbidisation from 40.2 and 67.9° (Pd (111) and (220) respectively) to 39, and 66.3°, a surprisingly small shift showing a small lattice expansion with no real change in symmetry. This lattice expansion has been followed in more detail using TPXAS, temperature-programmed X-ray absorption spectroscopy. As shown in Figure 2 the lattice expansion overall correlates well with the XRD result, with an expansion of 0.07 (±0.005) nm. However, it appears to proceed in two stages, with an expansion of ~0.015 nm up to about 100 °C, after which it expands much more up to completion at 180 °C. The small expansion at low temperature may be associated with the formation of adsorbed layers, which generally cause surface lattice expansions of up to ~10%.[20] This would lead to an average lattice expansion of ~0.001 nm, which is not far from what we observe. As the temperature increases, so the full lattice expansion is achieved as the bulk becomes saturated with C. Note that some sintering has occurred after many runs,

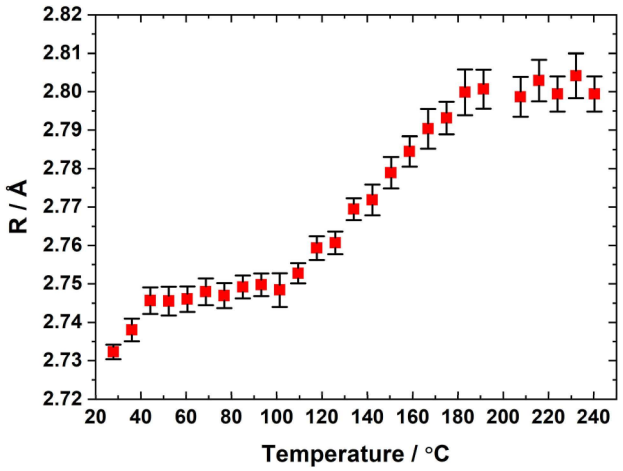

Figure 2. In situ measurements of the average lattice expansion of the Pd nanoparticles exposed to ethene as a function temperature of the sample.

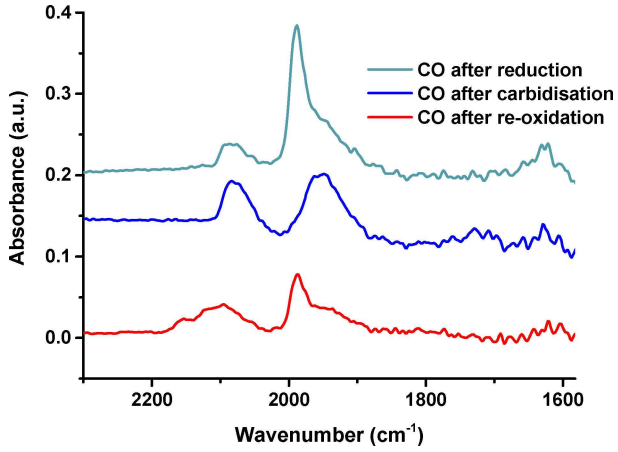

Figure 4. DRIFT spectra collected after CO adsorption at RT after each treatment stage, (Green-after reduction, Blue-after carbidisation on ethene exposure, Red-after re-oxidation).

with the average particle size in TEM increasing to ~9 nm (Figure S2b).

The exact cause of the lattice expansion can be determined by investigating the XANES region of the XAFS data (Figure 3). Pd hydride and Pd carbide have clear differences in their XANES spectra; both cause a negative shift in energy for the second XANES feature (~24390 eV), however, only the carbide gives rise to a broadening and a shift in energy (+1 eV) of the main edge transition.[7,17] When assessing the difference spectra (compared to metallic Pd) of the hydridic and carbidic forms of Pd there are clear features that allow us to easily distinguish between these interstitial structures; the Pd hydride difference spectrum has an intense peak at ~24360 eV, whereas the Pd carbide difference spectrum has a distinguishing peak at ~24374 eV (Figure 3a). By assessing the XANES difference spectra during our time-resolved XAFS studies (Figure 3b) we can assign the interstitial structure types at both stages of lattice expansion. XANES difference spectra at 69 °C and 224 °C both have an observable feature at 24374 eV, which allows us to assign that the lattice expansion in both cases is caused by Pd carbide formation. Indeed, this is consistent with the proposed hypothesis that the carbide phase is initially formed at the surface before diffusing into the bulk lattice.[8]

Turning to adsorption measurements, there is a significant change in the CO adsorption mode before and after such C dosing experiments seen by using *in situ* DRIFTS. As shown in Figure 4, the clean nanoparticles of Pd show the kind of CO spectrum seen by others,[21–23] with a major band at ~1990 cm^{-1}, proposed to be due to bridge-bonded CO, together with a lower intensity band at 2080 cm^{-1} (on-top) and broad shoulder on the high intensity band at ~1950 cm^{-1}, possibly due to bridge sites at the edge of particles.[24] Note that there appear to be no multiple bridge sites, which would be seen at much lower wavenumber (e.g. hollow 3-fold (111)

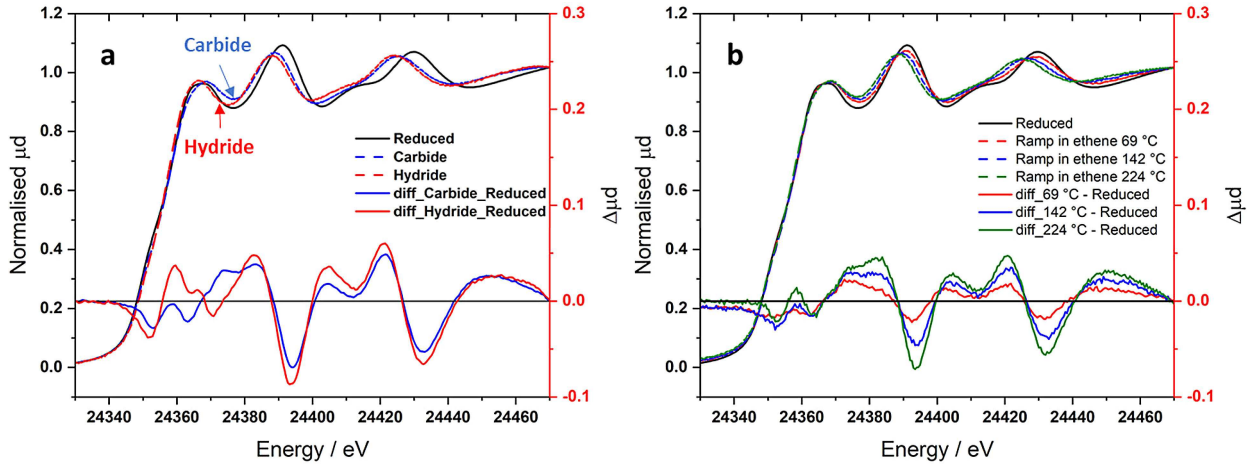

Figure 3. (a) Normalised Pd K edge XANES spectra of Pd^0, Pd hydride and Pd carbide. The difference spectra (−Pd^0 reference) of Pd carbide and Pd hydride are also shown. (b) Normalised Pd K edge XANES spectra during time resolved ethene decomposition (temperatures of 69 °C, 142 °C, 224 °C) alongside associated difference spectra.

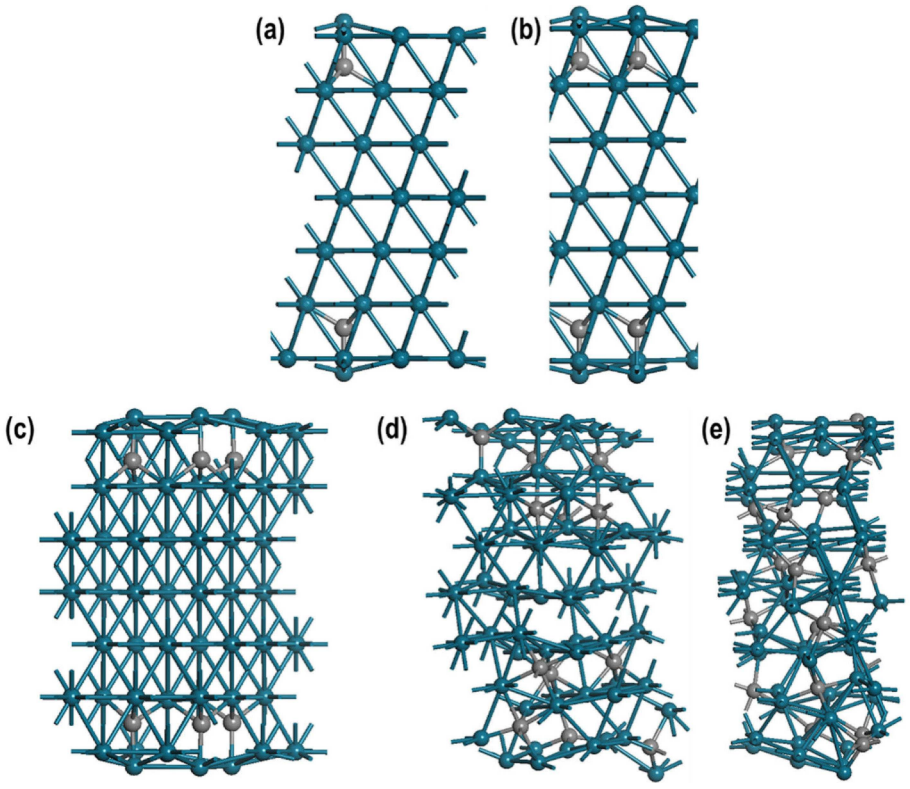

Figure 5. Pd(111) surface with (a) 2 C-atom (0.357 wt%), (b) 4 (0.711 wt%), (c) 6 (1.063 wt%), (d) 12 (2.105 wt%), and (e) 18 (3.124 wt%).

type sites). After carbidisation the main, clearly identifiable change is the loss of the 1990 cm^{-1} band, while the others remain, and after oxygen cleaning and removal, the original spectrum is largely restored, with some additional intensity in the 2130–60 cm^{-1} region due to CO–Pd^{+} species.[25] Evidently then, carbidisation has significantly altered the surface layers and blocked the bridge site adsorption.

We have also used density functional theory (DFT) to explore the expansion of Pd – Pd interatomic distances due to the presence of interstitial C atoms. For this study we included 0.357–3.124 wt% of interstitial carbon atoms in a 3×3 Pd model with 7 atomic layers (Figure 5). The calculated interatomic distances due to the presence of various concentration of interstitial C have been summarised in Tables 1–3. Our calculations show that in close proximity to the interstitial C-atom the Pd–Pd interatomic distance increases in the range of 0.007–0.042 Å, which show reasonable agreement with the experimental data. Additionally, we also calculate the charge transfer between the Pd and the interstitial C-atoms. There is an average

Table 1. Layer by layer Pd–Pd bond distances with increasing percentage of C atom intercalation.

C [wt%]	Pd–Pd bond distances Layer 1st	2nd	3rd	4th	Average
0.357	2.763	2.771	–	–	2.767
0.711	2.789	2.786	–	–	2.787
1.063	2.818	2.787	–	–	2.803
2.105	2.786	2.829	2.804	–	2.807
3.125	2.795	2.793	2.8238	2.797	2.802
C [wt%]	Difference w.r.t bulk Pd–Pd bond distance (2.760 Å) Layer 1st	2nd	3rd	4th	Average diff.
0.357	0.003	0.011	–	–	0.007
0.711	0.029	0.026	–	–	0.027
1.063	0.058	0.027	–	–	0.043
2.105	0.026	0.069	0.044	–	0.047
3.125	0.035	0.033	0.064	0.037	0.042

Table 2. Pd–Pd distance around the intercalated C atoms.

C [wt%]	Nearest Neighbour Av. Pd–Pd around C [Å]	Difference with bulk Pd–Pd bond distance [Å]	Av. Pd–C [Å]
0.357	2.816	0.056	1.909
0.711	2.823	0.063	1.911
1.063	2.825	0.065	1.936
2.105	2.828	0.068	1.985
3.125	2.830	0.070	2.007

Table 3. Average Bader charge on Pd and C atoms with increase in the number of interstitial C atoms.

Atoms	Average Charges 2	4	6	12	18
Pd	0.007	0.014	0.021	0.071	0.115
C	−0.210	−0.225	−0.224	−0.370	−0.402

change in Bader charge on the Pd of +0.007 e to +0.115 e, and on C between −0.210 e to −0.402 e (see Table S3). Effectively the radius of the Pd is decreased and the C increased, which may help to accommodate the C with relatively little overall expansion.

Conclusions

We have discovered that ethene not only dehydrogenates on nanoparticulate Pd supported on silica at above 200 °C, but concurrently it disproportionates to also produce palladium carbide and methane. We have found a higher level of carbidisation than previously reported by using chemical titration of the carbide with oxygen. The carbide formed is probably Pd_4C, but with minimal expansion of the Pd lattice, which we propose to be due to interstitial formation plus some charge transfer between Pd and C.

Experimental Section

Catalyst Synthesis

Pd catalysts supported on SiO_2 (Fumed 320–410 $m^2 g^{-1}$) were prepared using a sol-immobilisation method. An aqueous solution of K_2PdCl_4 of the desired concentration (9.39×10^{-4} M) was prepared in MilliQ water. To this solution polyvinyl alcohol (PVA) (1 wt% solution, Aldrich, averaged molecular weight MW = 9000–10000 g mol^{-1}, 80% hydrolysed) was added (PVA/Pd (wt/wt) = 0.65). Subsequently, a 0.1 M freshly prepared solution of $NaBH_4$ (> 96%, Aldrich, $NaBH_4$/Au (mol/mol) = 5) was then added to form a dark/brown sol. After 30 min of sol generation, the colloid was immobilised by adding SiO_2 (acidified to pH 1 by sulfuric acid) under vigorous stirring conditions. The amount of support material required was calculated so as to have a total final metal loading of 5% wt, but analysis of the filtrate indicated a loading of 4.4%. After 24 hours the slurry was filtered, the catalyst washed thoroughly with distilled water (1.5 L) and dried at 120 C for 8 hours. Finally, a calcination step was performed at 350 °C for 3 hours to remove the PVA.

The Reactor

Reaction measurements were carried out in a Hiden Catlab using its pulsed flow reactor capability.[26] 0.22 g of catalyst was loaded into the quartz reactor tube and heated in-situ prior to reaction to 250 °C in 10% H_2 in He, followed a pure He flow for one hour prior to the pulsing experiments. 10% Ethene in He was regularly pulsed over the catalyst every 2 mins and products analysed by on-line mass spectrometry. O2 (10% in He) could then be pulsed over the catalyst to remove the adsorbed/absorbed C.

XAFS-DRIFTS Measurements

XAFS measurements were performed at the Pd K-edge on the B18 beamline at the Diamond Light Source, Didcot, UK. Measurements were performed in transmission mode using a QEXAFS setup with fast-scanning Si (311) and (111) double crystal monochromators for the Pd edge. The time resolution of the spectra reported herein was 90s/spectrum (kmax = 12.5). A DaVinci arm fitted with Praying Mantis Optics was used to refocus the IR beam outside the FTIR spectrometer so that the X-ray beam could be transmitted through the DRIFTS cell. The samples were placed in the Harrick X-ray transmission DRIFTS cell attached to the end of the DaVinci arm. The arm has motorized stages able to move vertically and horizontally by 48 mm, enabling ease of alignment of the DRIFTS cell in the X-ray beam. The cell is fitted with glassy carbon windows for exit and entry of the X-ray beam and ZnSe windows for collection of DRIFTS spectra. The XAFS/ DRIFTS cell which has been described in detail elsewhere,[19] has an X- ray path length of 3.17 mm placed 1.04 mm below the surface of the catalyst. DRIFTS spectra were collected with an Agilent Carey 680 FTIR spectrometer taking 64 scans with a resolution of 4 cm^{-1} using the liquid nitrogen cooled MCT detector.

EXAFS (Extended X-ray Absorption Fine Structure) Analysis

All XAFS spectra were acquired concurrently with a Pd foil placed between It and Iref. XAFS data processing was performed using IFEFFIT[27] with the Horae package[28] (Athena and Artemis). Athena was used to calibrate, align, and normalize the spectra with respect to the Pd foil, for which E_0 was set at 24358 eV. EXAFS data processing of k2 data used an appropriate k range for the data (3.2−12.5 $Å^{-1}$). Analysis of the Fourier transformed data was limited to fitting with the first coordination shells using cif files of Pd. The amplitude reduction factor, S_0^2 was derived from EXAFS data analysis of the Pd foil reference spectra, (with known coordination numbers which were fixed during analysis). The value obtained was 0.85 for Pd, this value was used as fixed input parameters in the fits. The increase with temperature of the σ^2 value, the mean-square relative displacement of absorber and backscatter atoms, was estimated based on the method described elsewhere for the change in the σ^2 value with increasing temperature.[29]

While the EXAFS measurements showed an increase in Pd–Pd bond distance that is consistent with carbon absorption, it cannot directly measure the amount of carbon within the sample. Other X-ray techniques such as diffraction are also similarly hampered due to the strong scattering from Pd with respect to carbon.

Computational Details

We employed the Vienna Ab-initio Simulation Package (VASP) to perform DFT based calculations.[30–33] The projector augmented wave (PAW) method was used and the cut-off energy for the expansion of the plane-wave basis sets was set to 550 eV, which gave bulk energies converged to within 10^{-5} eV. We chose a convergence criterion of 0.01 eV/Å for our structural optimisations. For all the preliminary calculations, the most commonly used Perdew-Burke-Ernzerhof (PBE) version of the generalized gradient approximation (GGA) was used to carry out total energy calculations and perform geometry optimization.[34] The ideal Pd(111) surface was modelled by a 3×3 supercell with 7atomic layers with a theoretical lattice constant of 3.904 Å and a k-point grid of 3×3×1. During the optimization process, we relaxed the entire system, which consisted of interstitial carbon and the Pd(111) surface. In our models we placed the interstitial carbon atoms on the subsurfaces close to both sides of the exposed Pd(111) surface, which is to nullify the spurious dipole moments due to the presence of carbon atom on one side (Figure 1 (a–d). For all these calculations we also used Grimme's D3 corrections as dispersive effects in these systems may play a crucial role.[35] The charges on various atoms were obtained using the Bader charge analysis as implemented by Henkelman and co-workers.[36]

Acknowledgements

We are grateful to support from the UK Catalysis Hub, funded through EPSRC grants EP/I038748/1 and EP/K014714/1, and to the Research Complex at Harwell (RCaH) for provision of facilities.

Conflict of Interest

The authors declare no conflict of interest.

Keywords: Dehydrogenation · Disproportionation · Ethene · EXAFS · Palladium Carbide

[1] M. Bowker, R. Holroyd, N. Perkins, J. Bhantoo, J. Counsell, A. Carley, C. Morgan, *C. Surf. Sci.* **2007**, *601*, 3651–60.
[2] M. Bowker, C. Morgan, V. Zhdanov, *Phys. Chem. Chem. Phys.* **2007**, *9*, 5700.
[3] M. Bowker, L. Cookson, J. Bhantoo, A. Carley, E. Hayden, L. Gilbert, C. Morgan, J. Counsell, *Appl. Catal. A* **2011**, *391*, 394–399.
[4] M. Bowker, C. Morgan, N. Perkins, R. Holroyd, E. Fourre, F. Grillo, A. MacDowall, *J. Phys. Chem. B* **2005**, *109*, 2377–86
[5] S. B. Ziemecki, G. A. Jones, D. D. Swartzfager, R. L. Harlow, J. Faber, *J. Am. Chem. Soc.,* **1985**, *107*, 4547–8. J. Faber, *J. Am. Chem. SOC.* **1985**, *107*, 4547–4548, *Am. Chem. SOC.* 1107.
[6] A. L. Bugaev, O. A. Usoltsev, A. Lazzarini, K. A. Lomachenko, A. A. Guda, R. Pellegrini, M. Carosso, J. G. Vitillo, E. Groppo, J. A. van Bokhoven, A. V. Soldatov, C. Lamberti, *Faraday Discuss.* **2018**, *208*, 187–205.
[7] A. A. Guda, A. Lazzarini, K. A. Lomachenko, E. Groppo, R. Pellegrini, A. Piovano, H. Emerich, A. V. Soldatov, L. A. Bugaev, V. P. Dmitriev, J. A. van Bokhoven, C. Lamberti, *Catal. Today* **2017**, *283,* 119–126.
[8] A. L. Bugaev, O. A. Usoltsev, A. A. Guda, K. A. Lomachenko I. A. Pankin, Y. V. Rusalev, H. Emerich, E. Groppo, R. Pellegrini, A. V. Soldatov, J. A. van Bokhoven, C. Lamberti, *J. Phys. Chem. C* **2018**, *122*, 12029–37.
[9] D. Teschner, E. Vass, M. Hävecker, S. Zafeiratos, P. Schnörch, J. Sauer, A. Knop-Gericke, R. Schlögl, M. Chamam, A. Wootsch, A. S. Canning, J. J. Gamman, S. D. Jackson, J. McGregor, L. F. Gladden, *J. Catal.* **2006**, *242*, 26–37.
[10] M. A. Newton, M. Di Michiel, A. Kubacka, A. Iglesias-Juez, M. Fernμndez-García, *Angew. Chem. Int. Ed.* **2012**, *51*, 2363–2367; *Angew. Chem.* **2012**, *124*, 2413–2417.
[11] J. A. McCaulley, *J. Phys. Chem.* **1993**, *97*, 10372–10379.
[12] J. A. McCaulley, *Phys. Rev. B* **1993**, *47*, 4873.
[13] O. Balmes, A. Resta, D. Wermeille, R. Felici, M. E. Messing, K. Deppert, Z. Liu, M. E. Grass, H. Bluhm, R. van Rijn J. Frenken, R. Westerstrom S. Blomberg, J. Gustafson, J. N. Andersen, E. Lundgren, *Phys. Chem. Chem. Phys.* **2012**, *14*, 4796–4801.
[14] M. Maciejewski, A. Baiker, *J. Phys. Chem.* **1994**, *98*, 285.
[15] C. Chan, Y. Xie, N. Cailuo, Y. Yu, J. Cookson, P. Bishop, S. C. Tsang, *Chem. Commun.* **2011**, *47*, 7971–7973.
[16] M. W. Tew, M. Janousch, T. Huthwelker, J. A. van Bokhoven, *J. Catal.* **2011**, *283*, 45–54.
[17] M. W. Tew, M. Nachtegaal, M. Janousch, T. Huthwelker, J. A. van Bokhoven, *Phys. Chem. Chem. Phys.* **2012**, *14*, 5761–5768.
[18] M. Bowker, J. Counsell, K. El-Abiary, L. Gilbert, C. Morgan, S. Nagarajan, C. S. Gopinath, *J. Phys. Chem. C* **2010**, *114*, 5060–5067.
[19] E. K Dann, R. H. Blackmore, C. R. A. Catlow, P. Collier, A. Chutia, T. Erden, C. Hardacre, A. Kroner, M. Nachtegaal, A. Raj, S. A. Rogers, S. F. Taylor, P. Thompson, G. F. Tierney, C. Zelinapour-Yazdi, A. Goguet, P. P. Wells, *Nature Catalysis* 2019, 2, 157–163.
[20] G. A. Somorjai, an *Introduction to Surface Chemistry and Catalysis*, pp 89–91, Wiley Interscience, **1994**.
[21] J. B. Giorgi, T. Schroeder, M. Baumer, H.-J. Freund, *Surf. Sci.* **2002**, *498*, L71–L77.
[22] N. Sheppard, T. T. Nguyen in *Adv. Infrared Raman Spectrosc.*, Eds. R. J. H. Clark, R. E. Hester, (Heyden & Son: London) **1978**; *5*, 67–148.
[23] T. Lear, R. Marshall, J. Lopex-Sanchez, D. J. Jackson, T. Klapotke, M. Baumer, G. Rupprecter, H.-J. Freund, D. Lennon, *J. Chem. Phys.* **2005**, *123*, 174706.
[24] D. Tessier, A. Rakai, F. Bozon-Verduraz, *J. Chem. Soc. Faraday Trans.* **1992**, *88*, 741.
[25] K. I. Hadjiivanov, G. N. Vayssilov, *Adv. Catal.* **2002**, *47,* 307–511.
[26] S. Chapman, C. Brookes, M. Bowker, E. K. Gibson, P. P. Wells, *Faraday Discuss.* **2016**, *188,* 115.
[27] M. Newville, *J. Synchrotron Radiat.* **2001**, *8*, 322–4.
[28] B. Ravel, M. Newville, *J. Synchrotron Radiat.* **2005**, *12*, 537–41.
[29] W. Bohmer, P. Rabe, *J. Phys. C* **1979**,*12*, 2465
[30] G. Kresse, J. Hafner, *Phys. Rev. B* **1993**, *47*, 558–561.
[31] G. Kresse, J. Hafner, *Phys. Rev. B* **1994**, *49*, 14251–14269.
[32] G. Kresse, J. Furthmüller, *Comput. Mater. Sci.* **1996**, *6,* 15–50.
[33] P. E. Blöchl, *Phys. Rev. B* **1994**, *50,* 17953–17979.
[34] J. P. Perdew, M. Burke, M. Ernzerhof, *Phys. Rev. Lett.* **1996**, *77*, 3865–3868.
[35] S. Grimme, J. Antony, S. Ehrlich, H. Krieg, *J. Chem. Phys.* **2010**, *132*.
[36] W. Tang, E. Sanville, G. Henkelman, *J. Phys. Condens. Matter* **2009**, *21*, 84204.

Manuscript received: April 30, 2019
Revised manuscript received: June 11, 2019
Accepted manuscript online: June 17, 2019
Version of record online: July 26, 2019